

Boundary Layer Model to Account for Thick Mask Effects in PhotoLithography

Jaione Tirapu-Azpiroz^a, Paul Burchard^b and Eli Yablonovitch^a

^a Electrical Engineering Department, UCLA

^b Mathematics Department, UCLA

Los Angeles 90095-1594

E-mail: jaione@ee.ucla.edu, eliy@ee.ucla.edu

phone: 1 310 206 3724, 1 310 206 2204

ABSTRACT

The lack of transparent optical components at short wavelengths limits the available wavelengths in Deep Ultraviolet lithography, while the required minimum feature on wafer continues to shrink towards deeper sub-wavelength scales. This places a serious limitation on Kirchhoff boundary conditions that replace the field on the mask openings by the incident field, since this approximation fails to account for the increasingly important topographical effects (thick mask effects) in the computation of the lithographic image. In this paper we present a sophisticated version of Kirchhoff approximation capable of modelling rigorous near field effects while retaining the simplicity of the scalar model. Our model is based on a comparison of the fields produced by both the thick and ideal thin masks on the wafer. Polarization and edge diffraction effects as well as phase and transmission errors, are included in our model.

Keywords: Thin mask model, Phase-shifting Masks, Aerial image simulation, Kirchhoff Boundary Conditions, Deep Ultraviolet Lithography

1. INTRODUCTION

In the past few years, the lithographic process entered for the first time into the *subwavelength* regime of operation. This means that the minimum feature of the printed circuit on wafer is smaller than the wavelength of the light source, limited to 157nm by the lack of refractive lenses in Deep Ultraviolet Lithography (DUVL). Several sophisticated extensions of binary masks have been progressively added over the last decade, such as Phase Shifting Masks (PSM), to enhance resolution while reducing the printable Critical Dimension (CD). Simulation of aerial image formation however, relied entirely on Kirchhoff Boundary Conditions to approximate the field immediately behind the patterned mask with an equivalent scalar binary model (Thin-mask approximation). The advantageous simplicity of the Kirchhoff model allows fast, yet reasonably accurate calculations for feature sizes much larger than the source wavelength, but turns out very inaccurate at sub-wavelength dimensions where topography effects arising from the vector nature of light become noticeable¹⁻⁴.

Some of these thick-mask effects: polarization dependence due to the different boundary conditions for the electric and magnetic fields, transmission error in small openings, diffraction edge effects or electromagnetic coupling, become particularly critical for Alternating Phase-Shifting masks (Alt. PSM) since they are based on the modulation of both amplitude and phase of the em field propagating through them. Consequently, resource-consuming rigorous 3D electromagnetic field simulations have become necessary in aerial image formation of an Alt PSM mask, raising the demand for accurate but still simple physical models.

Some examples of modeling methodologies have been explored in the literature for both Deep and Extreme Ultra-Violet (EUV) Lithography. In the DUV regime, Adam and Neureuther^{5,6} followed an approach that replaces the rigorous em field on the aperture by a "scalar complex mask transmission function" that best matches the complex diffraction pattern of the near field in its lowest spatial frequencies. Their procedure speeds up the calculations while providing good accuracy⁶, but it is limited to square or rectangular features.

Yan's approximation⁷ of diffraction effects on the absorber edges of 2D EUVL line patterns by adding a strip to the thin mask model provides another type of model, more suited for local application irrespective of the overall geometry. Both Yan's and our approach share the possibility of locally modeling topographical mask effects with a boundary band of different transmission coefficient at the thin mask edges. However, in the two approaches, slightly different procedures are followed to determine the layer width and transmission parameters.

In Yan's approach, the width and transmission coefficients of the boundary layer were directly obtained by matching correctly the diffraction ripples of the near field evaluated on the mask surface. For the 3D DUVL transmission masks analyzed in this paper, we performed a systematic study of imaging rectangles of different aspect ratios and selected the boundary layer parameters to optimize the central field amplitude on the wafer, not the mask.

The boundary layer model replaces the thick mask with the customary thin mask, adding only a fixed-width, locally-determined boundary layer to every edge. Boundary layers are already employed in industry to account for the losses in peak intensity of the field traveling through small apertures in the chromium mask, but always in the form of a bias, that is, an opaque boundary layer. In contrast, our imaginary boundary layer model added to Kirchhoff approximation allows modeling of thick mask effects, different polarizations, and accounts for phase errors on the aerial image by permitting a complex transmission coefficient in the boundary layer area.

The next few paragraphs will describe in detail the Boundary Layer (BL) model proposed in this paper for a typical Alternating Phase-Shifting mask while section 3 will focus on the methodology for obtaining the model parameters (width and transmission coefficient). Finally, efficiency and accuracy aspects will be discussed in section 4.

2. BOUNDARY LAYER MODEL PARAMETERS

Scalar diffraction theory relying on the Kirchhoff approximation replaces the mask by an ideal transmission function and neglects polarization and edge diffraction of the real mask. Multiplication of the incident field times this transmission function yields the object field on the exit surface of the mask, and its Fourier Transform constitutes the far field or aerial image that impinges on the thin lens. Under the thin lens assumption, the imaging system is equivalent to a low-pass filter collecting only the region of the near field diffraction spatial frequencies that lie inside its collection cone (Numerical Aperture), and that will contribute to the wafer image. In this fashion, the electric field on the wafer produced by a thick phase shifting mask is compared against that produced by its corresponding thin mask model.

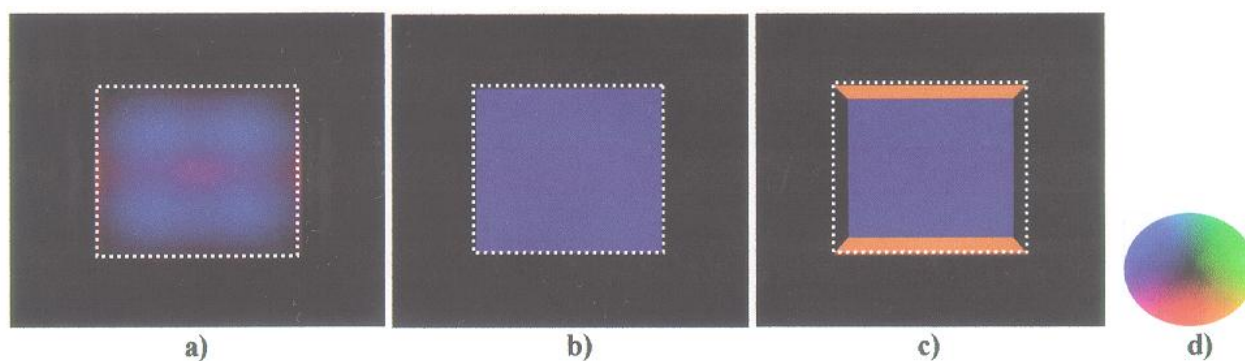


Figure 1. a) Sketch of the actual field calculated by FDTD on the aperture of a 744 nm 180°-shifter square opening with horizontally polarized electric field. b) Kirchhoff scalar approximation (thin mask model) of the field on the same aperture. c) Imaginary Boundary Layer model for the same square opening and illumination. d) Scale of complex numbers normalized to unity.

The Boundary Layer width and transmission coefficients collected in table 1 for the three types of openings utilized in Alt. PSM lithography, correspond to the material parameters and exposure conditions given in table 2 and 3, respectively. Usually, the width of the boundary layer adjusts the variation in peak amplitude, while the imaginary transmission coefficient corrects phase deviations of the scalar case. These errors differ for different types of mask edge cross-sections, giving different boundary layer parameters. Moreover the model presents the advantage of being locally applied in the vicinity of the edges, allowing us to extend it to complicated geometries.

Figure 1(a) shows a plot of the actual electric field immediately below an square 180° -phase-shift opening on a thick chrome mask of 744nm (3λ with $\lambda = 248nm$) side with horizontally polarized incident electric field, as evaluated by a Finite Difference Time Domain algorithm, Tempest 5.0². This rigorously calculated field on the aperture exhibits standing wave patterns, physically sensitive to the illumination orientation with respect to the metal edges, that are neglected by the conventional thin mask model of the same feature as depicted in figure 1(b). The efficiency of the conventional Kirchhoff approximation for openings much larger than the wavelength motivated the search for a scalar complex model retaining much of the Kirchhoff simplicity such as that displayed on figure 1(c), corresponding to our imaginary boundary layer model applied to the same 3λ 180° -phase-shift square opening and horizontally polarized incident light.

Notice the direction dependence of the boundary layer transmission coefficient that reaches its maximum value when the electric field is tangent to the boundary, and diminishes to zero when the field is normal to it. This simple geometric rule (cosine rule) accounts for the orientation dependence of the boundary conditions at the metal edges. Tangential components of the electric field must vanish on metal surfaces, setting up conditions for standing-wave effects on the aperture field that contribute to the phase errors. Normal electric field components, on the other hand, exhibit a discontinuity due to the accumulation of charges on the chrome surface, but its contribution to the final projected image is mostly filtered out by the optical lens⁸.

Table 1.
Width and transmission coefficients of the boundary layer model
for different type of openings in typical PSM geometry

Opening type	Boundary Width(nm)	Tangential Boundary Transmission	Normal Boundary Transmission	Interior Transmission	Minimun opening(nm)
Clear	25.2	0.0i	0	1	248
Shifter	52	-0.53i	0	-1	300
Shifter with 35nm undercut	37.5	-0.66i	0	-1	350

In order to compare both the amplitude and phase of the field on the wafer produced by the rigorously calculated field on the mask and its corresponding thin mask and Boundary Layer models, the wafer image was generated by an imaging system consisting of a 4X reduction lens of Numerical Aperture equal to 0.68. Results for 180° -phase-shift square openings illustrated in figure 3(a) of sizes equal to 1.2λ , 1.8λ and 3λ are shown in figures 2(a)-(c), respectively. They reveal a close agreement between the images generated by both the exact field (solid line) and its Boundary Layer model (dashed line) in both amplitude and phase plots, what yields to a remarkable reduction of the error caused by the conventional Kirchhoff approximation (dash-dot line). Moreover, this agreement extends throughout the range of opening sizes and aspect ratios analyzed, providing good agreement in amplitude and phase errors no larger than 5 degrees for the smallest sizes.

Illumination in industrial applications consists of an unpolarized source of partially coherent light, what in practice requires separate results for both orthogonal (TE and TM) polarizations to be incoherently superposed. We treated the illumination as coherent, and at normal incidence. According to Hopkin's approximation,⁸ this is valid for 4X reduction systems within a cone angle of 3.5° in air.

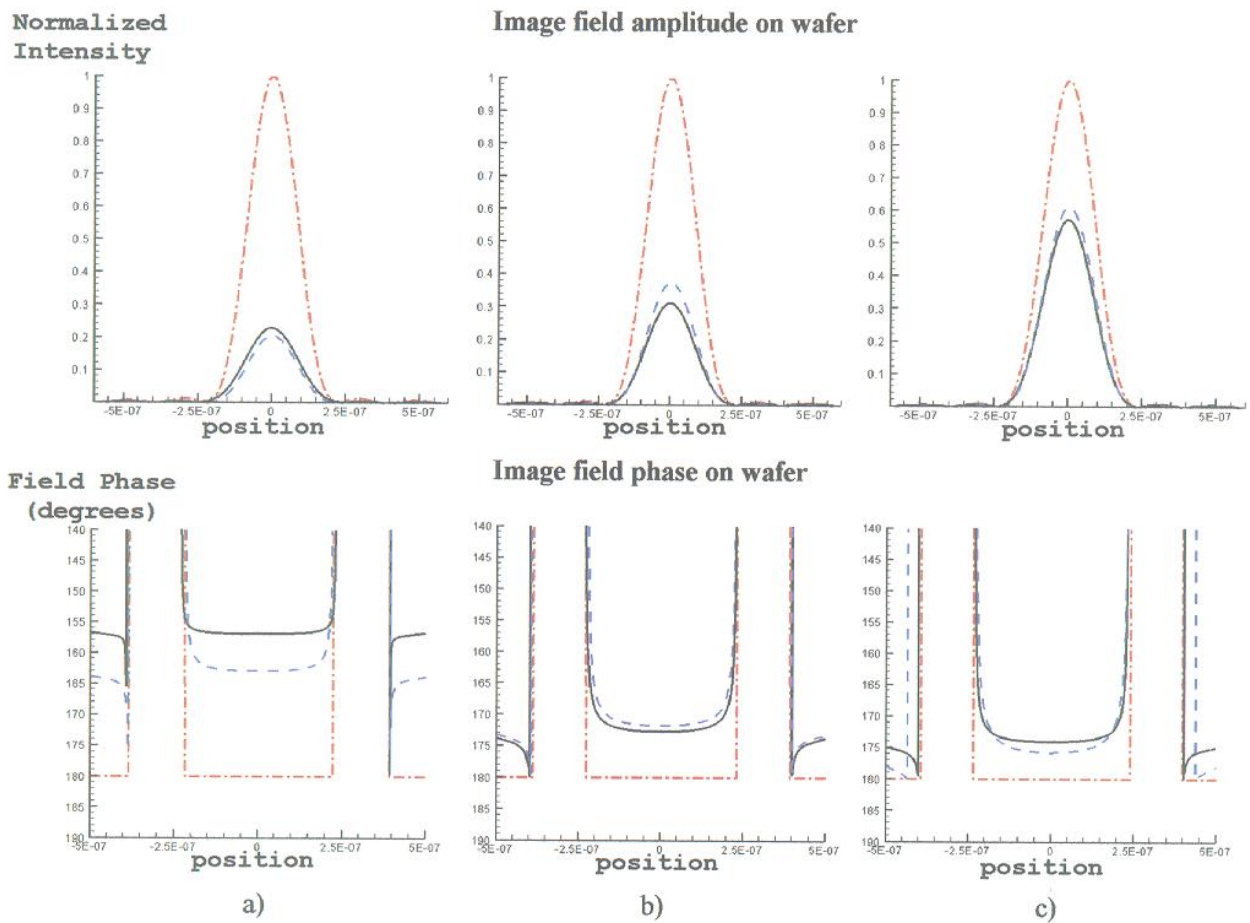


Figure 2. Comparison of both amplitude and phase of the wafer images produced by the exact field at the aperture (solid) and both its corresponding Kirchhoff approximation (dash-dot) and Boundary Layer model (dashed), for three different sizes of 180°-phase-shift square opening: a) 1.2 λ, b) 1.8 λ and c) 3 λ, respectively.

3. BOUNDARY LAYER PARAMETERS DETERMINATION

TABLE 2: Mask parameters and rectangular opening ratios and sizes

Chrome layer	Thickness=80nm Refractive index n=2.5 Extinction coeff. k=2
Glass layer	Refractive index n=1.5
Opening sizes	248nm (λ) to 1488nm (6λ)
Rectangular Opening ratios and sizes	3:1, 3:2, 2:1, 1:2, 2:3, 1:3 for minimum sizes equal to 248nm to 496nm

TABLE 3: Exposure conditions

Light source	wavelength = 248nm Coherent illumination Normal incidence
Polarization	Linear along x
NA	0.68
Lens reduction	0.25

The boundary layer parameters are based on the comparison of the electric field on the wafer produced by a various thick phase-shifting masks against that produced by their corresponding ideal thin mask models. Rigorous electromagnetic results for the thick masks were obtained from 3D Tempest simulations performed with a grid of 40 nodes per wavelength (more than twice as fine as recommended) to ensure accuracy. Coherent, on-axis illumination of 248 nm wavelength, linearly polarized on the horizontal direction was employed. The thick mask simulation patterns consisted of single rectangular openings with side sizes ranging from 1 to 6 wavelengths, aspect ratios ranging from 3:1 to 1:3, and three different etching profiles per shape: 0° , 180° shifter and 180° shifter with 35 nm undercut, as illustrated in figure 3(a). Finally, the chrome layer was assumed to be 80 nm thick with a refractive index of $2.5-2j$ at 248 nm, and 1.5 for glass at the same frequency⁴. The etching depth for the 180° shifter-opening equal to the vacuum wavelength. As mentioned in section 2, the electric field on the wafer is obtained via the Fourier Transform of both the exact and the modeled near fields, followed by a 4X reduction lens of Numerical Aperture equal to 0.68. Tables 2 and 3 summarize the mask material parameters and exposure conditions, respectively, while figure 3 shows a cross section plot of the mask geometries analyzed in this paper together with the aperture fields they generate.

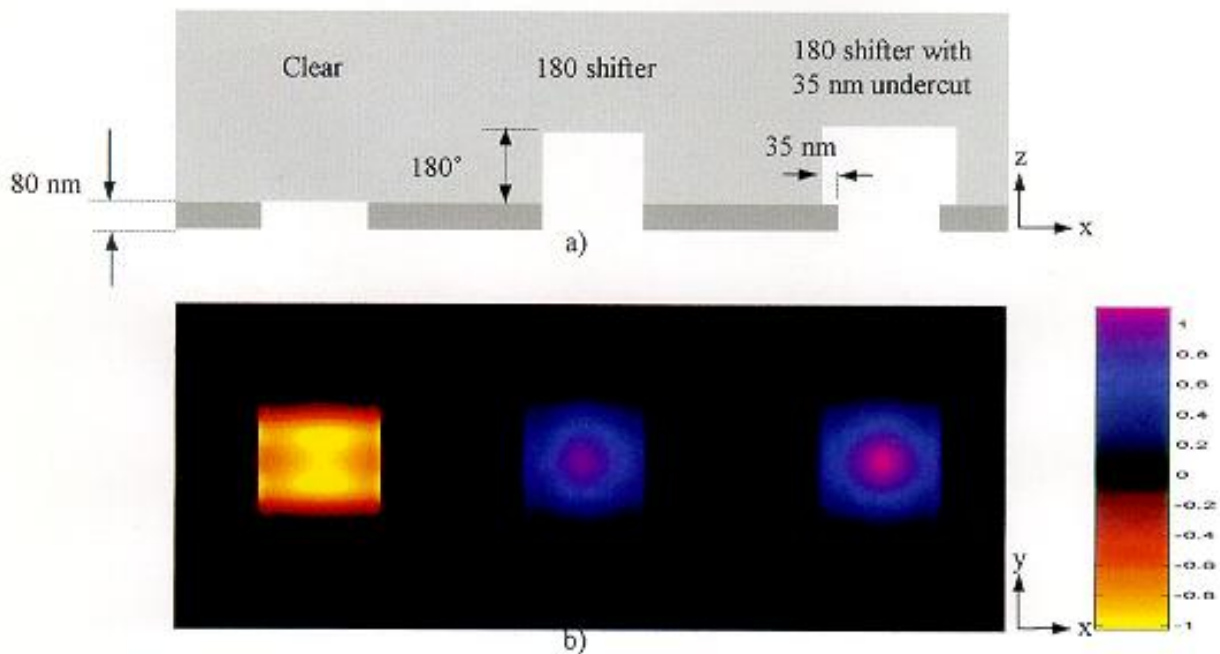


Figure 3. a) Sketch of the three types of openings on a transmission lithography mask. b) Aperture field generated by each opening.

3.1. Relative Error in Amplitude

The electric field amplitude on the wafer produced by the thin mask model has a purely real magnitude, either positive or negative for unetched or etched apertures, respectively. The relative error in the electric field amplitude on the wafer produced by this thin mask approximation is therefore measured by the deviations of its real component from the rigorously FDTD calculated em field value, and plotted in figure 4(a) for the range of openings previously indicated. It was observed that this amplitude deficit at the wafer follows a nice

inverse law in the size of the opening, not only for square features but also for all aspect ratios of rectangular openings analyzed, as long as the opening size is measured as the harmonic mean of its width (w) and its height* (h). The harmonic mean indicates that the relative error in amplitude due to Kirchhoff approximation can be assumed proportional to a correction width, Δd , to be applied on all four sides of the thin mask model independently of polarization and that, as outlined in equation (1), this correction width can be assumed uniform independent of the size of the opening.

$$\text{Relative Error} = \frac{\text{Electric Field Error}}{\text{Total Electric Field}} = \frac{\Delta \mathbf{E}}{\mathbf{E}} = \frac{4\Delta d}{d} = \frac{4\Delta d}{\frac{2wh}{w+h}} = \frac{(2w+2h)\Delta d}{wh} = \frac{\text{Boundary Layer Area}}{\text{Total Area}}. \quad (1)$$

Equation (1) indicates that the harmonic mean results in a fixed boundary layer width, and figure 5(a) shows the real part of the Boundary Layer model, where an opaque layer of zero transmission is placed on all four sides of the opening to account for amplitude errors.

Weighting the width and height unequally or combining them by a formula other than the harmonic mean produced a poorer fit to the inverse law. It was noticed, however, that while the unetched openings follow the inverse law all the way down to the smallest sizes simulated (one wavelength), the etched openings (shifter and shifter with 35 nm undercut) deviated from the inverse law below 400 nm, exhibiting higher than expected transmission.

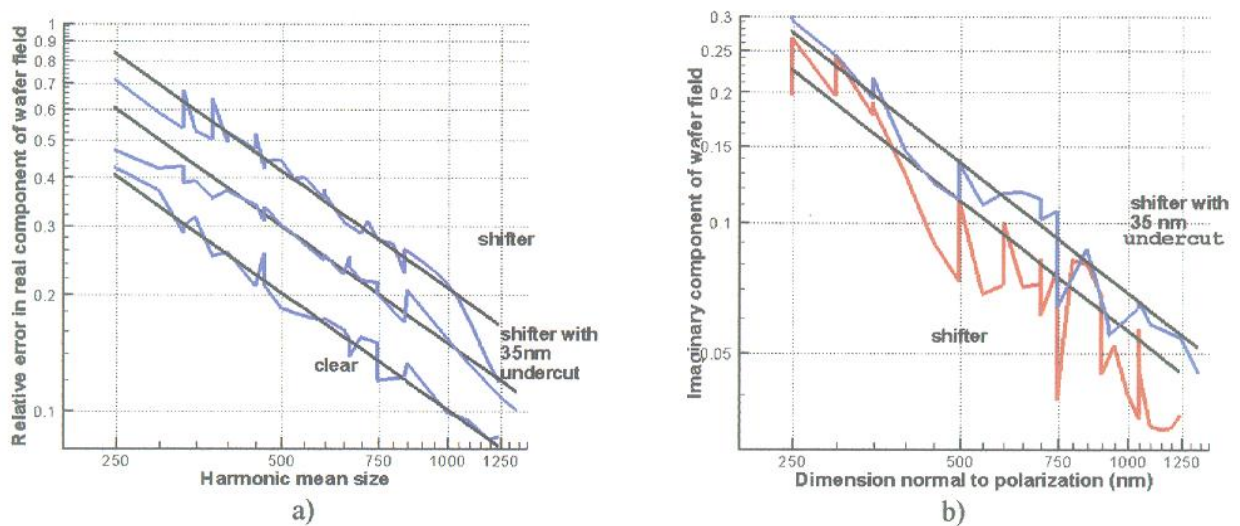


Figure 4. a) Log-log plot of the relative error in the real component of the electric field on the wafer produced by the thin mask approximation as compared to the rigorously evaluated EM field versus the harmonic mean of the opening height and width. b) Log-log plot of the relative error in the imaginary component as a function of opening height (opening size in the direction perpendicular to polarization).

3.2. Relative Error in Phase

Because any non-zero value of imaginary part of the field at the wafer relative to the thin mask field indicates a phase deviation from the ideal 0 or 180 degrees, relative errors of phase were analyzed by plotting the

*Harmonic mean is defined as: $\frac{2}{\left(\frac{1}{h} + \frac{1}{w}\right)}$

imaginary field component versus the opening height. This dimension is defined as the side length in the direction perpendicular to the electric field polarization and it turned out that the same inverse law in this dimension holds for all square and rectangular openings of all aspect ratios. Any other functional dependence of the error such as the reciprocal of the dimension parallel to polarization, produced a much poorer inverse law fit. Hence, the conclusion that the Boundary Layer has a purely imaginary transmission coefficient, $-j\beta$, that is proportional to the absolute value of the cosine angle between the electric field polarization and the edge direction, arises directly from the dependence in figure 4(b) formulated in equation (2),

$$\text{Relative Imaginary Error} = \frac{\text{Im}\{\Delta\mathbf{E}\}}{\mathbf{E}} = \beta \frac{2\Delta d}{h}. \quad (2)$$

The best fitting straight line to the collected data provided the actual value of this transmission coefficient, needed to compensate for phase deviations of the field and to determine the imaginary part of the Boundary Layer model as plotted in figure 5(b). Only the etched mask profiles yielded nonzero imaginary coefficients since phase errors for unetched openings were too small to show systematic variations.

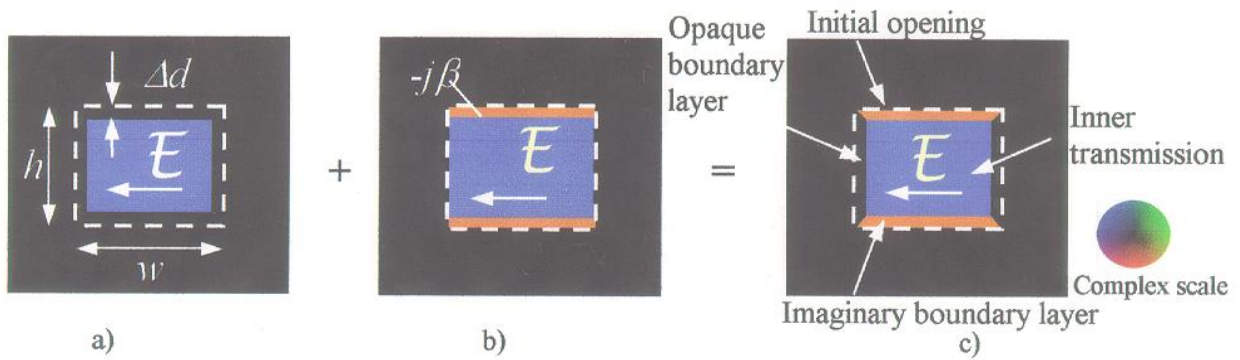


Figure 5. a) Real component of the Boundary Layer model. b) Imaginary component of the Boundary Layer model. c) Final Boundary Layer model as the superposition of both real and imaginary parts.

Finally, the superposition of both real and imaginary parts of the model give the final Boundary Layer as sketched in figure 5(c), with the parameters of width and transmission coefficient outlined in Table 1. The boundary layer parameters were obtained, for each etching profile, from the slope of the best fitting straight line to the data points, in a least squares sense.

Note that a slightly different set of parameters could have been obtained by allowing the boundary layer to take complex values rather than being purely opaque or with an imaginary transmission coefficient. Requiring purely imaginary boundary layer transmission leads to the simplest type of model yet providing satisfactory results in terms of root mean square errors of the field on the wafer.

4. ROBUSTNESS AND EFFICIENCY

Since the lithographic industry utilizes photomask pattern designs with features comparable to the illumination wavelength, in an attempt to push the limits of optical resolution, rigorous simulation of mask topographic effects become necessary. In practice, however, the numerical effort required to evaluate Maxwell equations on even relatively small mask areas is too high and reliable modelling of these thick mask effects has turned out to be challenging.

The robustness of our model relies on the fact that all amplitude and phase effects of the thick mask can be reduced to just two fixed parameters: width and transmission coefficient of the boundary layer. Moreover,

these parameters turn out to vary in a reasonable way with the etch profile and provide lower errors for the field on the wafer even for mask features close to the wavelength as observed in the plot in figure 6 of the root mean squared error (RMS).

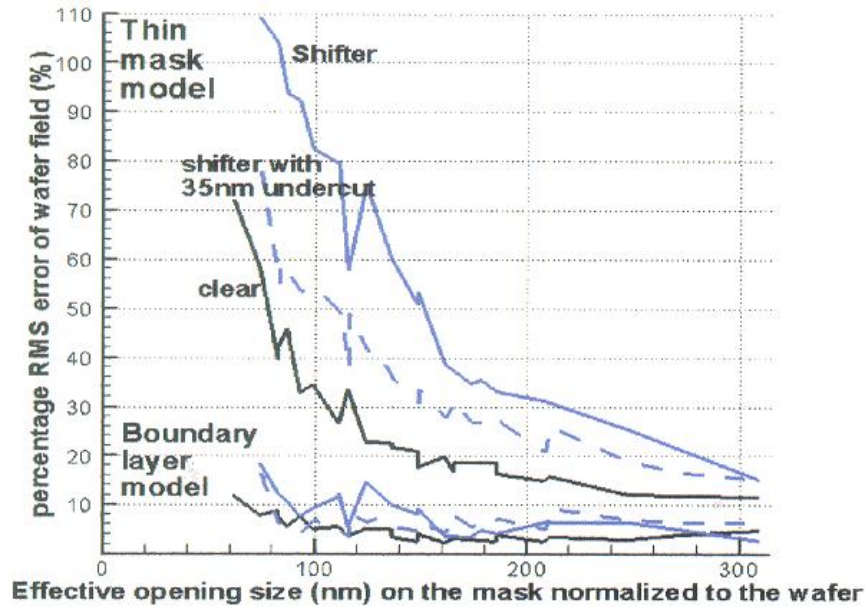


Figure 6. Root mean squared error on the projected image on the wafer for both the conventional thin mask and the boundary layer model of the set of rectangular apertures collected in Table 2.

Although the thick mask effects decay slowly with the size of the opening, the key result of our simulations is that this decay can be interpreted, to a good approximation, as a locally determined, fixed-size edge effect, what can increase the overall efficiency of the image calculation.

5. CONCLUSIONS

A new boundary layer model is proposed to improve the accuracy of aerial image computation in photolithography simulations based on binary thin mask scalar approximations. Unlike the models relying simply on Kirchhoff approximation, the boundary layer model incorporates topographic effects and polarization dependencies of the field transmitted by the photomask. We observed how the relative errors of the real and imaginary field components on the wafer follow an inverse law on the opening mean size and height, respectively. This allowed us to model them as a simple boundary layer of fixed width and transmission coefficient. Numerical evaluation of the rms error on the wafer images produced by rectangular openings proved an improved agreement between rigorously evaluated em fields and scalar models when an appropriate Boundary Layer is added to the feature edges. In this fashion, a localized application of the boundary layer model to larger and more complex mask domains will allow accurate simulations at reasonable computational cost.

ACKNOWLEDGMENTS

The project described was supported by grant number DAAD19-99-1-0196 from U.S. Department of the Army, a subaward from the University of New Mexico and by the "La Caixa" Foundation Scholarship Program (Spain).

REFERENCES

1. M. S. Yeung and E. Barouch, "Limitation of the kirchhoff boundary conditions for aerial image simulation in 157 nm optical lithography," *IEEE Electron Device Lett.* **21 No 9**, pp. 433–435, Sep. 2000.
2. A. K. Wong and A. R. Neureuther, "Rigorous three-dimensional time-domain finite-difference electromagnetic simulation for photolithographic applications," *IEEE Trans. on Semiconductor Manufacturing* **8, No 4**, pp. 419–431, Nov. 1995.
3. D. G. Flagello and A. E. Rosenbluth, "Lithographic tolerances based on vector diffraction theory," *J. Vac.Sci.Technol.* **B10(6)**, pp. 2997–3003, Nov/Dec 1992.
4. A. K. Wong and A. R. Neureuther, "Mask topography effects in projection printing of phase-shifting masks," *IEEE Trans. on Electron Devices* **41, No 6**, pp. 895–902, 1994.
5. T. V. Pistor, K. Adam, and A. R. Neureuther, "Rigorous simulation of mask corner effects in extreme ultraviolet lithography," *J. Vac. Sci. Technol.* **B 16 (6)**, pp. 3449–3455, Nov/Dec 1998.
6. K. Adam and A. R. Neureuther, "Simplified models for edge transitions in rigorous mask modeling," *Proc. of the SPIE* **4346 pt.1-2**, pp. 331–344, 2001.
7. P.-Y. Yan, "Understanding bossung curve asymmetry and focus shift effect in euv lithography," *Proc. of SPIE* **4562**, pp. 1–9, 2001.
8. G. Wojcik, J. J. Mould, R. Ferguson, R. Martino, and K. K. Low, "Some image modeling issues for i-line, 5x phase shifting masks," *Proc. of the SPIE* **2197**, pp. 455–465, 1994.